Bridge-piling modifications on the momentum balance in an estuary: The role of tides, winds and seasonality

Carmen Zarzuelo [a,*], Arnoldo Valle-Levinson [b], Alejandro López-Ruiz [a], Manuel Díez-Minguito [c], Miguel Ortega-Sánchez [c]

[a] Departamento de Ingeniería Aeroespacial y Mecánica de Fluidos, Universidad de Sevilla, Camino de los Descubrimientos s/n, 41092, Seville, Spain
[b] Department of Civil and Coastal Engineering, University of Florida, 365 Weil Hall, P.O. Box 116580, Gainesville, FL 32611, USA
[c] Andalusian Institute for Earth System Research, University of Granada, Avda. del Mediterráneo, s/n, 18006 Granada, Spain

ARTICLE INFO

ABSTRACT

Marine structures modify the hydrodynamics in relatively shallow coastal areas such as bays and estuaries, as analyzed here in the Bay of Cádiz. This study explores the momentum balance and the wakes generated by bridge piles, through a validated numerical model of a well-mixed mesotidal estuary. Three main drivers are considered: tides, winds and buoyancy forcing. The results show that the contribution of advection has the same order of magnitude as that of the barotropicity, with baroclinicity being relevant only during summer. The effects of the pile are intensified inside the basin (i.e., the bay) during spring-tides and ebb periods, and outside the bay during neap-tides and flood periods. These changes in the momentum balance reach up to 1 km landward in the deepest areas and up to 2 km seaward in the shallowest areas. The momentum terms vary the most in spring and summer, when wind forcing is weak. Westerly winds coinciding with flood-tide periods increase the advection in the outer basin, because of the pile. In contrast, easterly winds coinciding with the ebbing tides intensify the advection in the inner basin. Results can be extrapolated to other study sites with similar human interventions such as wind or wave energy converters.

1. Introduction

Estuarine environments act as sources and sinks of water and sediment, through the exchange of fluxes with different densities (Hamilton, 1990). In estuaries, hydrodynamic behavior is mainly determined by the following factors (Jay and Smith, 1990; Thurman, 1981; Sumich and Morrissey, 1996; Janzen and Wong, 2002; Stark et al., 2017b,a, 2019): (i) tides; (ii) winds; (iii) estuarine morphology and geometry; and (iv) freshwater input(s). The combination of these five factors has a profound impact on water quality, residual sediment dynamics, and, consequently, on their morphodynamic evolution (Zhang et al., 2018).

Population increases around estuarine environments (Seas and Plans, 2011) have resulted in effort to facilitate the expansion of urban areas (like bridges or motorways among others) and to improve their economic activities (such as widening ports or new navigation channels; Fernández-Fernández et al., 2019; Zarzuelo et al., 2015, 2019a,b; Velasquez-Montoya et al., 2020). Moreover, increases in marine resource exploitation (Pisacane et al., 2018) have resulted in developing new infrastructures such as wind farms and tidal energy converter arrays. The structures associated with such arrays can give rise to

vortices that affect the estuarine turbulent kinetic energy (Grashorn and Stanev, 2016). In turn, this turbulence alters surface flows and water column stratification (Dorrell et al., 2022), while generating ecological impacts that threaten species and habitats in the vicinity of the constructions (Lloret et al., 2022). Environmental interventions also alter the water-column stratification (Lass et al., 2008; Alahmed et al., 2021). The impacts of the interventions on the stratification are more evident in shallow waters, where two zones can be distinguished within the estuaries: (1) areas of exchange between water masses with different salinities, and (2) zones where other forcings such as winds are important in the baroclinic circulation (Dorrell et al., 2022).

The impact of changes in energy fluxes on estuarine dynamics, and the direction and magnitude of velocities caused by the wakes at the side of obstacles, have been analyzed through idealized numerical and experimental models (Cazenave et al., 2016; Grashorn and Stanev, 2016). In these studies, the impact of obstacles has consistently focused on quantifying the energy balance, and analyzing the turbulence and vorticity caused by outflow through an obstacle. Still to determine are the tidal variations in the momentum balance triggered by the obstacle

in a natural setting, and the influence of the dynamics on water column stratification. Moreover, in contrast to smaller structures such as wind farms or tidal energy converters, the bridge-piling modifications are more complex due to the size of the obstacle, as it can be large enough to modify the exchange of water and sediment between ocean and sea. This type of intervention has received scarce attention in estuaries (Miller and Valle-Levinson, 1996; Zarzuelo et al., 2021), and the few existing studies focus on observations of the effect on tidal dynamics. However, there are no studies analyzing how bridge piles can modify stratification and exchange fluxes of material, or determining the tidal, synoptic, and seasonal variability of such fluxes as impacted by the piles.

An example of an estuary where bridge-piling can alter the hydrodynamics is the Bay of Cádiz (southwestern Spain), a well-mixed mesotidal estuary where the interaction between tidal driver, complex geometry, and longitudinal density gradient generates complex dynamics. These dynamics have been studied by Zarzuelo et al. (2015, 2017), who also have explored the morphodynamics and the fate of the tidal creeks within the bay without considering the effect of human actions (Zarzuelo et al., 2018, 2019a). The impact of human interventions on the hydro-morphodynamics of the bay, specifically the dredging of the navigation channel and the extension of the terminal, has been analyzed by Zarzuelo et al. (2020). More recently, Zarzuelo et al. (2021) studied the effect of the bridge pile, focusing on observations at a cross-section adjacent to the bridge (Fig. 1). Two field surveys were carried out in this section that analyzed the tidal currents, and the effects of the bridge pile on the tidal dynamics. However, remaining is the study of the local impact of the piles on the momentum balance, as well as the extent of the generated wakes, their temporal variability, and their effect on water-column stratification.

The objectives of this work are to determine the effect of the bridge pile (Bay of Cádiz) on the momentum balance at different temporal scales (tidal, synoptic and seasonal) and their possible effect on water-column stratification. This analysis allows the assessment of the pile-induced changes in the forces that dominate the exchange. The work is focused in the vicinity of the bridge, which adds complexity through its geometry and its engineering modifications. The area of influence of the bridge pile merits particular focus for the changes observed in Zarzuelo et al. (2022).

The calibrated and tested three-dimensional DELFT3D model is used to achieve these objectives. The modeling approach allows resolution of the relevant physical processes at different spatial scales. Simulations of tidal currents, water levels and densities provide information for the momentum balance estimates as influenced by the pile. Results can be extrapolated to other human interventions involving one or several obstacles in the propagation of the tidal wave (e.g., wind or wave energy converters, isolated or in farms). The paper is structured as follows: after the description of the study area in Section 2, the methodology used is presented in Section 3, followed by the methodology used for interpretation of the results in Section 4. The discussion in Section 5 presents the main advances and issues, followed by brief conclusions (Section 6).

2. Field study

The Bay of Cádiz is an estuarine system in the south-southwestern Iberian Peninsula (36 ° 23'–36 ° 37'N, Fig. 1). It has an extension of 140 km^2, and is composed of three areas: (a) the outer basin, 70 km^2 and open to the ocean, with gentle slopes and mean depths of 10 m, and the discharge of two rivers (Guadalete and San Pedro); (b) the Puntales Channel (3.8 and 1.3 km long and wide, respectively) that connects the outer with the inner basins, characterized by steep slopes and maximum depths of up to 18 m; and (c) the inner basin, with the shallowest depths and an extension of 50 km^2. This inner basin reconnects with the sea through the Carracas and Sancti-Petri tidal channels (Zarzuelo et al., 2019a, 2020).

Freshwater discharges have a relatively weak influence on the Bay dynamics given their ≤ 20 m^3/s mean values. The estuary is dynamically short (compared to the tidal wavelength) and predominantly tidally driven (Zarzuelo et al., 2017, 2020). The amplitudes of the four predominant tidal constituents M2, S2, K1, and O1 are 1.03, 0.37, 0.68, and 0.67 m respectively, and the tidal form factor is approximately 0.96, thus it is a mixed semi-diurnal tide with a mean tidal range from 2 to 4 m (Zarzuelo et al., 2015). Mean tidal flow velocities vary from 1 to 1.5 m/s (Zarzuelo et al., 2015). Hourly data at buoy 2342 (6.96 ° W, 36.48 ° N, panel a- Fig. 1, Puertos del Estado, Spanish Ministry of Transport, Mobility and Urban Agenda) for the period 1996–2022 indicate that the winds are predominantly westerly and easterly. Their respective maximum speeds are 22 m/s and 20 m/s, with average values of 8.3 m/s and 10.1 m/s (Fig. 1).

Over the last two decades, the Bay of Cádiz has had two main human interventions: the expansion of the Port of Cádiz, including a dredging of $3.86 \cdot 10^6$ m^3 of sediment, and the aforementioned bridge. Both the port and the bridge have affected the hydrodynamics and morphodynamics of the estuary. Puntales Channel (Fig. 1, zone B) is the most intervened, and the site of the new bridge "Constitución 1812". This study concentrates on the impacts of the "Constitución 1812" bridge. The bridge has a length of 5 km and a height of 69 m above mean sea level. It has 7 piles of 20 x 20 m located at a depth of 5 m, and a large central pile of 60 x 60 m located at a depth of 15 m. While Zarzuelo et al. (2015, 2019a) have studied how such interventions affect the hydrodynamics and morphodynamics of the Bay, the focus was on the effects derived from the harbor expansion and the dredging of the navigation channel. Zarzuelo et al. (2022) studied the influence of the central pile of the bridge (since the rest interfered with the hydrodynamics by less than 2%) and how it modified the tidal flows. Therefore, this study focuses on a small part of the estuary (area B- Fig. 1a), where there is a uniform width (transverse: 1.3 km, longitudinal: 8 km) and a constant depth (10–15 m) (Fig. 1-d).

3. Methodology

3.1. Numerical model

Process-based numerical simulations were used to analyze the spatial and temporal scales of the momentum balance terms, as they change due vary with different drivers such as tide or wind. Moreover, the wake extension caused by the piling has been assessed at tidal, synoptic and seasonal scales. The flow module of the open-source Delft3D software (WL| Delft Hydraulics) solves the shallow water equations with the Boussinesq approximation, using finite volume methods on staggered unstructured grids. The vertical schematization for the 3D simulations implements a σ-layer scheme with a fixed number of layers. The 3D simulations, together with the model's heat fluxes module (Zarzuelo et al., 2021), provide the water density fields necessary to analyze the effect of the wakes on stratification. Based on previous results (Zarzuelo et al., 2015, 2021, 2022), the model has been used in its hydrostatic version as the vertical motions are negligible (e.g. Mahadevan et al., 1996a,b; Marshall et al., 1997). Nonhydrostatic versions of unstructured grid ocean models are viable for solving higher frequency and smaller scale cases of both surface and internal wave motions (e.g. Fringer et al., 2006; Lai et al., 2010; Wang et al., 2011; Zhang et al., 2011).

The model has been implemented using a grid that covers the entire Bay of Cádiz, including the three areas defined in section , as well as the tidal channels (Fig. 1, b). The unstructured grid consists of 90405 cells in plan. It has a spatial resolution of 200 x 200 m^2 in greater depths and up to 60 x 60 m^2 near the influence of the bridge (Zarzuelo et al. 2022). This discretization allows defining the pier section as a drypoint, where the velocity at the centroid of the cell is set to zero and no flux is permitted through the cell side boundaries. The vertical grid layout has been defined with a total of 10 cells (their thickness are
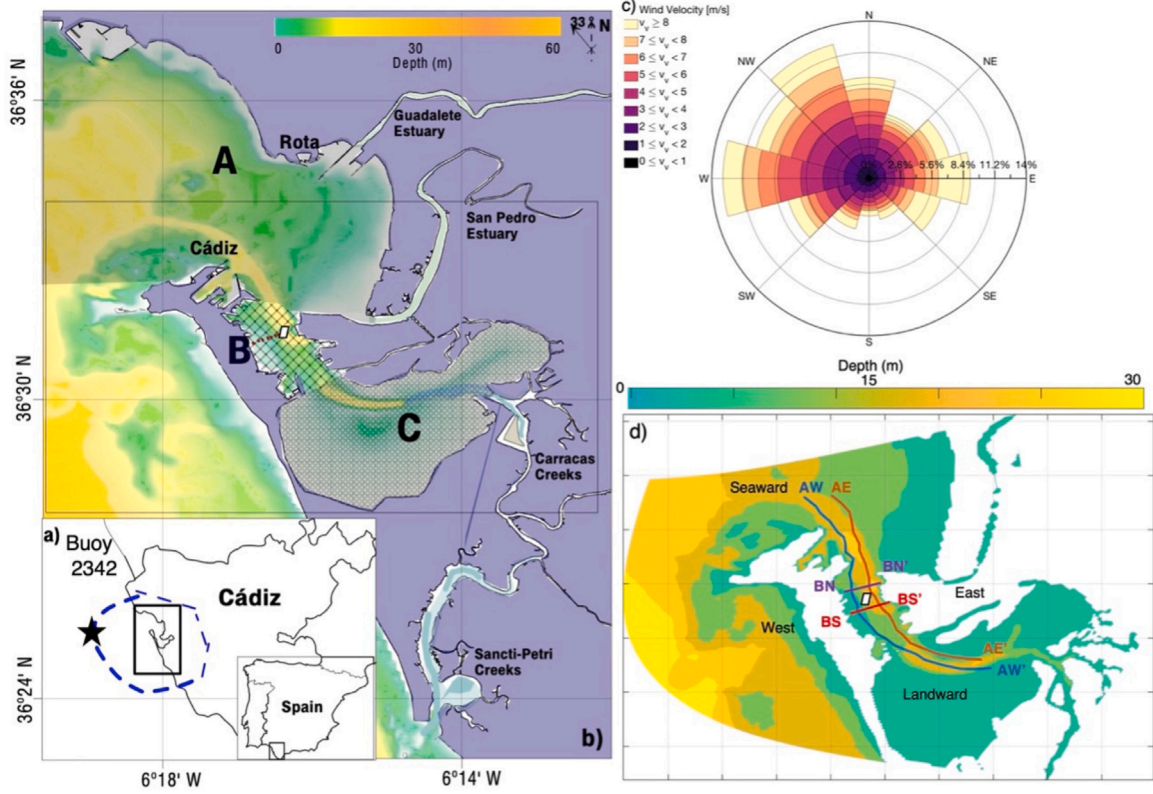
Fig. 1. Panel a: location of the Bay of Cádiz (Spain), the mesh (blue dashed line) of the Delft3D model; panel b: location and detail of the three areas of the Bay of Cádiz; panel c: the wind rose of the Buoy 2342; panel d: longitudinal profiles (West and East, blue and orange AW-AW' and AE-AE', respectively) and cross-sections (Seaward and Landward, purple and red BN-BN' and BS-BS', respectively). The bridge pile is highlighted with a white rectangle in panels b and d.

2, 10, 10, 10, 10, 10, 10, 10, 10, 2% of the water depth). Starting from the grid defined in Zarzuelo et al. (2021), the geometry of the grid has been adapted to define the bridge pile as a cell with no mass transport through its walls, following Zarzuelo et al. (2022).

The model has been forced with water level boundary conditions corresponding to 18 tidal constituents obtained in Cádiz with spatial variability derived from TPOX 8.0 (Egbert and Erofeeva, 2002). In addition, a spatially uniform time-varying wind field has been defined throughout the spatial domain with hourly data from Buoy 2342 (Fig. 1-a). To calculate the atmosphere/ocean heat exchange at regional scale, daily data of solar radiation, temperature, humidity, and cloudiness have been provided by the regional government of Andalusia (Spain). The data described above as well as the setup of the model used can be found in Zarzuelo et al. (2021), which also describes the calibration and validation process through observations at sites near the bridge pile using free surface, velocities, temperature, and salinity in 2D and 3D (Zarzuelo et al., 2019a, 2021, 2022).

Previous simulations performed in the study area, where the mesh was refined inside the bay and in the creeks, and all modules were fine-tuned including hydrodynamic and heat fluxes, were used to analyze (1) the role of wave and heat exchange between different areas of the bay (Zarzuelo et al., 2021) and (2) modifications on tidal-flow due to the bridge pile (Zarzuelo et al., 2022). However, these works did not characterize the wakes generated by the bridge piles and their impact on the momentum balance near the pile.

3.2. Momentum balance

Along- and cross-channel momentum balance terms are described by (West–East and Seaward–Landward, respectively Fig. 1) (Geyer and MacCready, 2014):

$$\rho H \frac{\partial u}{\partial t} = -\rho H \left(u \frac{\partial u}{\partial x} + v \frac{\partial u}{\partial y} \right)$$
$$- g\rho H \frac{\partial \xi}{\partial x} - \frac{g}{\rho_0} \rho H \int_z^\xi \frac{\partial \rho}{\partial x} dz - \rho H f v + \rho H \frac{\partial}{\partial z} \left(A_z \frac{\partial u}{\partial z} \right) \quad (1)$$

$$\underbrace{\rho H \frac{\partial v}{\partial t}}_{\text{Local}} = \underbrace{-\rho H \left(u \frac{\partial v}{\partial x} + v \frac{\partial v}{\partial y} \right)}_{\text{Advective}}$$
$$\underbrace{- g\rho H \frac{\partial \xi}{\partial y}}_{\text{Barotropic}} \underbrace{- \frac{g}{\rho_0} \rho H \int_z^\xi \frac{\partial \rho}{\partial y} dz}_{\text{Baroclinic}} \underbrace{+ \rho H f u}_{\text{Coriolis}} + \underbrace{\rho H \frac{\partial}{\partial z} \left(A_z \frac{\partial v}{\partial z} \right)}_{\text{Friction}} \quad (2)$$

where H is the total depth, being equal to $h + \xi$ (water depth plus water level). x, y and z represent the along-, cross-estuary and vertical coordinates, respectively. u and v indicate the along- and cross-channel velocities. The density perturbation $\rho' = \rho - \rho_0$ with respect to the mean value ρ_0 (1025 kg/m³).

The left-hand side of the equations is the local acceleration component. On the right side the first term is the horizontal advective term, the second and third represent the barotropic and baroclinic pressure gradient, respectively, the fourth term is Coriolis which will be neglected because it is minimal compared to the rest of the terms (Rossby number $Ro = U/fB > 1$, where B the width of the basin and U is the residual velocity along-channel) and the fifth term is the friction term, represented by the vertical mixing of momentum, where A_z is the vertical eddy viscosity. The vertical advection terms are neglected because they are much smaller than the horizontal advection terms.
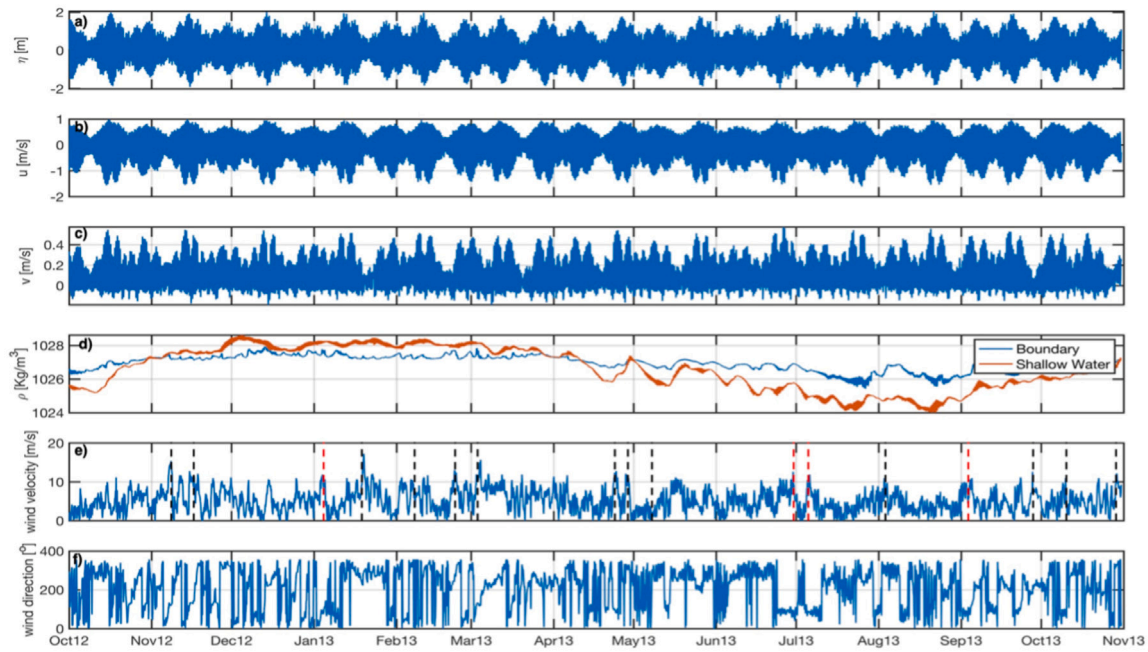
Fig. 2. Tidal conditions and climate forcings during the simulation period (September 2012–October 2013). From top to bottom: Times series of (a) water level, (b) east velocity, (c) north velocity measured in the outer basin, (d) density measured in the Buoy 2342 (blue line) and in the outer basin (orange line), (e) wind speed and (f) wind direction.

The changes produced on the vertical are minimal compared to the average in 2D as seen in previous studies (Zarzuelo et al., 2015, 2022). Thus, to assess the relative roles of momentum fluxes, Valle-Levinson and Schettini (2016) and Juarez et al. (2020) introduced the non-dimensional analysis of the depth-integrated momentum balance equations using numerical data. The residual advective and baroclinic terms, defined as tidal-cycle average, were obtained applying a low pass filter to the time series, removing the fluctuations at semi-diurnal and higher frequencies (De Jonge, 1992).

3.3. Design of numerical experiments

According to the objectives previously described, two cases have been simulated for the same boundary and forcing conditions and simulation period: the first represents present conditions (with bridge pile) whereas the second corresponds to the geometry of the before the bridge construction (no pile). Fig. 2 shows the tidal conditions and climate forcings observed at one point in the outer Bay (Fig. 1b) and the climate forcings (buoy 2342) during the simulation period (October 2012–October 2013), coincident with the sampling period described in Zarzuelo et al. (2022) and representing an average year without extreme forcings. Within the climate forcings only the wind is analyzed since the wave climate, as seen in Zarzuelo et al. (2019a), does not play a relevant role in the morphodynamics of the inner Bay. The month corresponding to September 2012 was simulated but will not be considered in the analysis because it was used for model spin up. Maximum spring tides are observed with tidal ranges of up to 4 m, with minimum values in neap tides of 1 m (Fig. 2a). Flow speeds reach maximum values of 1.5 m/s (Fig. 2b and c). An increase in water density is observed in the winter months (1029 kg/m^3) with a decrease of 5 kg/m^3 in summer (Fig. 2d). In addition, the seasonal variation is more pronounced in the inner bay (shallow water). Finally, four peaks of maximum wind speeds of 15 m/s (black dashed line- Fig. 2e) are observed, coinciding with westerly winds (Fig. 2f). Only three relevant events with easterly winds of 10 m/s were observed in January 2012, July 2013 and September 2013 (red dashed line- Fig. 2e).

The momentum balance is analyzed at four time scales: (1) yearly averaged conditions, (2) tidal variability, including fortnightly and

subtidal scales, (3) seasonal variability and (4) event scale for extreme wind conditions. The effects of the pile are quantified by analyzing simulations with and without the pile. These analyses, except for the stratification conditions, are carried out in 2D (horizontal, depth-averaged), along two along-channel profiles (West and East ($L = 10$ km), blue and orange, respectively, Fig. 1c) and two cross-channel profiles (Seaward and Landward ($W = 1.5$ km), blue and orange, respectively, Fig. 1d) located in the vicinity of the pile.

3.4. Dimensionless numbers

To support the discussion of the momentum balance equation, two dimensionless numbers are calculated: the turbulence intensity and the strain-induced periodic stratification (SIPS) number. The turbulence intensity is used to verify the zone of influence of the pile at tidal scale, and the SIPS number is used to verify the changes found over the baroclinic term.

Turbulent wakes behind obstacles such as bridge piles or wind farms help to identify and limit the zone of influence (King and Johns, 1976) of these structures. An increase in vortices, similar to those known as von Kármán vortices, can be related to the intensity of turbulent kinetic energy (TKE, e.g., Grashorn and Stanev, 2016). The barotropic pressure gradient in this case study is much greater than the baroclinic contribution (Zarzuelo et al., 2022), in contrast to other studies (Southern California Bight, Dong et al., 2007; Dong and McWilliams, 2007). The time-averaged turbulence intensity is calculated as $I = u'/U_{M2}$, where $u' = \sqrt{2/3k}$, k is the simulated time-averaged TKE per unit mass and U_{M2} is the semi-major axis of the surface M2 tidal current (Flórez-Orrego et al., 2012).

Tidal stirring will oppose the development of stratification on the ebb and accelerate its breakdown on the flood. A condition for the occurrence of significant Strain-Induced Periodic Stratification (SIPS, Burchard and Hetland, 2010) is described by Simpson's number which analyzes the dependence of the horizontal density gradient on the presence of longitudinal currents. Simpson's number is calculated as $Si = -g(\Delta\rho)/dx * \rho_0 h^2/(C_d \cdot U_{M2}^2)$, where the variation of $\Delta\rho$ was calculated with the maximum deviation of the densities along each station coincident with a maximum ebb. During ebb, the horizontal

density gradient interacts with the vertical shear of the current, causing a stable structure (Simpson et al., 1990). However, the reverse may occur during flood phases (Nepf and Geyer, 1996).

4. Results

In the following, the changes in the amplitude of the momentum terms will be analyzed at different time scales. Furthermore, some additional results not directly related with the main aim of this research are showed in the Supplementary Material, such as the analysis of the directional spreading of the flow field after the pile construction.

4.1. Averaged condition analysis of the momentum balance

Changes in the momentum balance caused by the bridge pile are calculated through the relative differences (pile - no pile/pile) of the mean and standard deviation of each term. These calculations are assessed over the entire simulated year along the four transects defined (Figs. 3 and 4).

The terms that have the greatest influence on the dynamics are the advective (b) and barotropicity (c), being at least twice as high as the rest (see Supplementary Material for additional results representation). In the case of the along-channel profiles (Fig. 3) the largest changes (95%) are found Seaward of the pile. The advection (b) modifies up to more than 2 km Seaward, and the friction (e) term up to 4 km Seaward. Close to the pile, there is an increase on the advective term, which is balanced by friction. These changes are more noticeable in the case of the East profile, with an increase in the terms close to the pile while decreasing when moving away from it. Also, the Landward zone has similar behavior than Seaward, being the main difference that the baroclinicity (d) loses importance in favor of friction (e). A noteworthy is the change, up to 90%, in the baroclinicity (d) in the inner bay 3 km Landward from the pile, where the section widens, and the depths decrease (Landward). The local term shows minor changes in both along- and cross-channel profiles.

In the cross-channel profiles (Fig. 4), the highest rates of variation occur in the same terms, almost up to 85%. Both East and West of the pile, the terms that increase (due to the pile) are the barotropicity (c) and friction (e) which are balanced by the advection (b). At 600 m from the pile on the western margin, the balance increases the advective (b), barotropic (c) and friction (e) terms, with the effects being balanced by the baroclinic (d) term. In the shallower western margin areas, the only term that increases is the advective, decreasing the effects of the pile by the baroclinicity (d). In both the Seaward and Landward cross-channel profiles, the behavior is similar, except in the area close to the pile (200 m) and in the shallower areas that behave in the opposite way. Moreover, the mass fluxes between west and east bank, and seaward and landward have been analyzed to see the exchange between fluxes, looking at where the net mass flux moves to (for more detail see the Supplementary Material).

4.2. The role of the pile on the tide-driven momentum balance

To examine the tidal variability, the momentum equations pressure terms (absolute terms) are analyzed in Figs. 5 and 6 at fortnightly scales over one year. The results obtained from the advection and barotropicity are shown, as they represent almost 85% of the force balance. In addition, the baroclinicity is shown because of its importance at seasonal scales. The local and friction terms are not shown, as they only represent 5% of the variance. As shown in the previous sections, the largest terms are the advection and barotropicity, being their values between 2 and 3 orders of magnitude higher than the rest.

The longitudinal profiles (Fig. 5) show that the advective (b) and barotropic (c) terms increase with the spring tides, up to values of 3 Pa. On the along-channel profile West (Fig. 5-1, running through the shallowest zone), the highest values are concentrated in the outer

basin (Seaward, higher depths) and around the bridge pile up to a length of 2 km Landward for the advection (b.1), and up to almost 3 km in the barotropic (c.1). In the along-channel profile East (Fig. 5-2), the highest values are concentrated in the constriction zone as it opens into the inner basin (Landward, around the kilometer 6) for the advection (b.2) as this is where the highest velocities are found. Moreover, there are changes around kilometer 3 (at the connection of the outer with the Puntales Channel) in the case of the barotropicity (c.2). The baroclinicity (d) (as seen in the previous section) is less than half that of the advection and barotropicity.

An analysis of the cross-channel profiles (Fig. 6) shows similar patterns to those described above. The highest values are found for both advection and barotropicity in the eastern margin (deeper zone). Particularly, in the cross-channel profile Seaward (Fig. 6-1), the advective term (b.1) gains importance in spring tides, being relevant throughout the section. However, in neap tides it only dominates in the eastern margin. In the case of the barotropicity (c.1), a relationship with the tidal variation is observed, being more relevant near the pile on spring tides and on the margins on neap tides. For the cross-channel profile Landward (Fig. 6-2) the behavior is reversed from the previous one; in this case, the advective term (b.2) is important only at the eastern margin, at spring tides throughout and at neap tides only at the margin. And the barotropic term (c.2), in spring tides is in almost all the relevant section, however the term is only more relevant in the East margin in neap tides.

The effect of the pile on the observed changes in tidal variability are analyzed in Figs. 7 and 8. The green–yellow colors indicate an increase with the construction of the bridge pile, and the blue colors a decrease. In the longitudinal profile, the most significant changes are observed at spring tides (almost 80%). In the case of the advective term, the effects reach up to 500 m in the along-channel profile West (70%, Fig. 7b.1) and up to 2 km in the along-channel profile East (Fig. 7b.2) Seaward (with the pile increases 60%). Landward, the effect of the pile is noticeable up to almost 2 km (with the pile it decreases by almost 40%). The barotropic term is similar, with Seaward changes being more noticeable on the along-channel profile West (150%, Fig. 7c.1) than on the along-channel profile East (120%, Fig. 7c.2). The eastern longitudinal section (Fig. 8) exhibits further modifications due to its higher depths and because it is where the highest velocities are concentrated (Zarzuelo et al., 2015, 2018). The baroclinicity (Fig. 8d) is hardly modified by the pile.

Remaining to explore is the effect of the flood–ebb tide periods, where changes are found exclusively in the velocities as seen in Zarzuelo et al. (2015, 2021). The largest changes occur on the West compared to the East margins at neap tides. These results are in agreement with the differences between the projected velocities on the channel axis, which are concentrated in the West margin during an interval of maximum flood at neap tides (Fig. 9a). Changes are also observed in the eastern margin, although with less intensity. This is because, during an interval of maximum ebb (Fig. 9b), such changes are concentrated Landward of the East margin. These results indicate that, since the pile acts as an obstacle, it modifies the direction of the along-channel velocities, increasing them up to 30%, and generating wake vortices. In turn, the changes produced in the East longitudinal profile are greater than those in the West, since, as observed by Zarzuelo et al. (2018), the ebb currents are 20% higher than the flood currents. These results highlight the impact that these obstacles have on the hydrodynamics of estuarine environments. Despite being a single pile, its effects extend distances ≥ 1 km (both Seaward and Landward) and correspond to surface areas that, in this case, exceed 2.5 km^2 (47% of the Puntales Channel).

4.3. The role of the pile on seasonal variations in momentum balance

Figs. 5–8 indicate seasonal variability. In both along-channel profiles the highest values are in the summer, from Jun 13 to Oct 13,
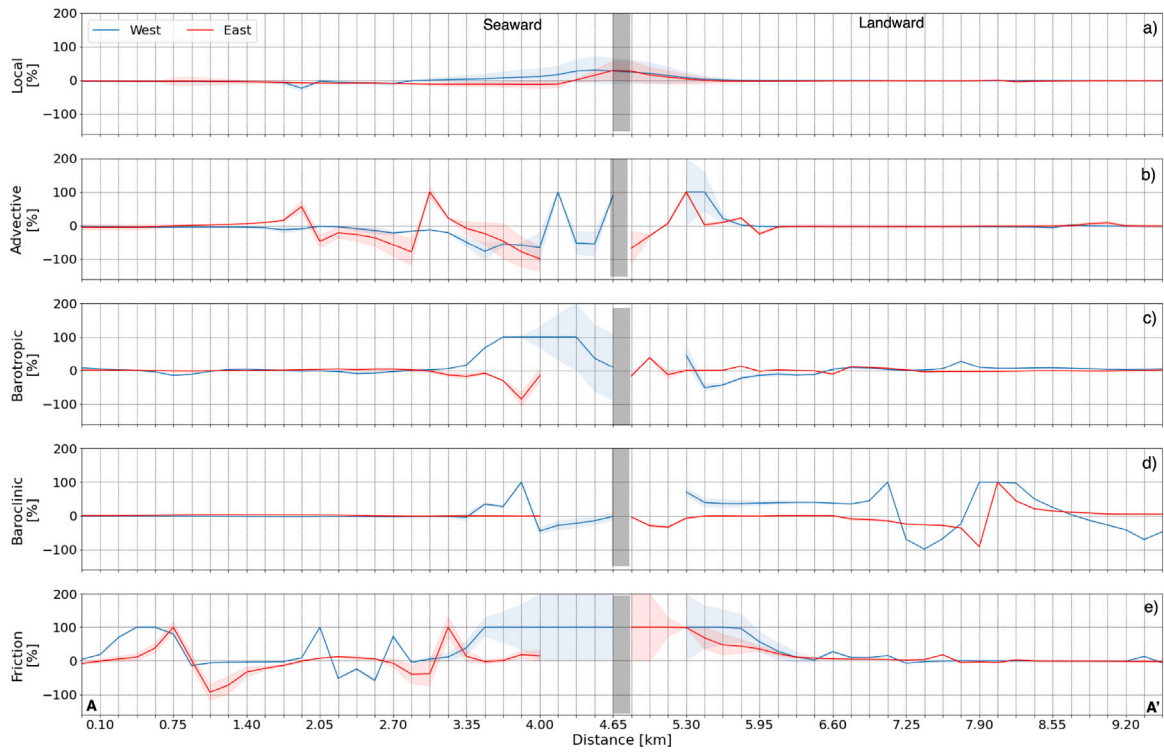
Fig. 3. Variation of the mean (solid line) and deviation (filled) over the whole simulated year of the local pressure (a), advective (b), barotropic (c), baroclinic (d), and friction (e) terms for the West (blue) and East (red) along-channel profile, for the relative differences between simulations (pile-no pile/pile · 100). The vertical black rectangle represents the location of the bridge pile.
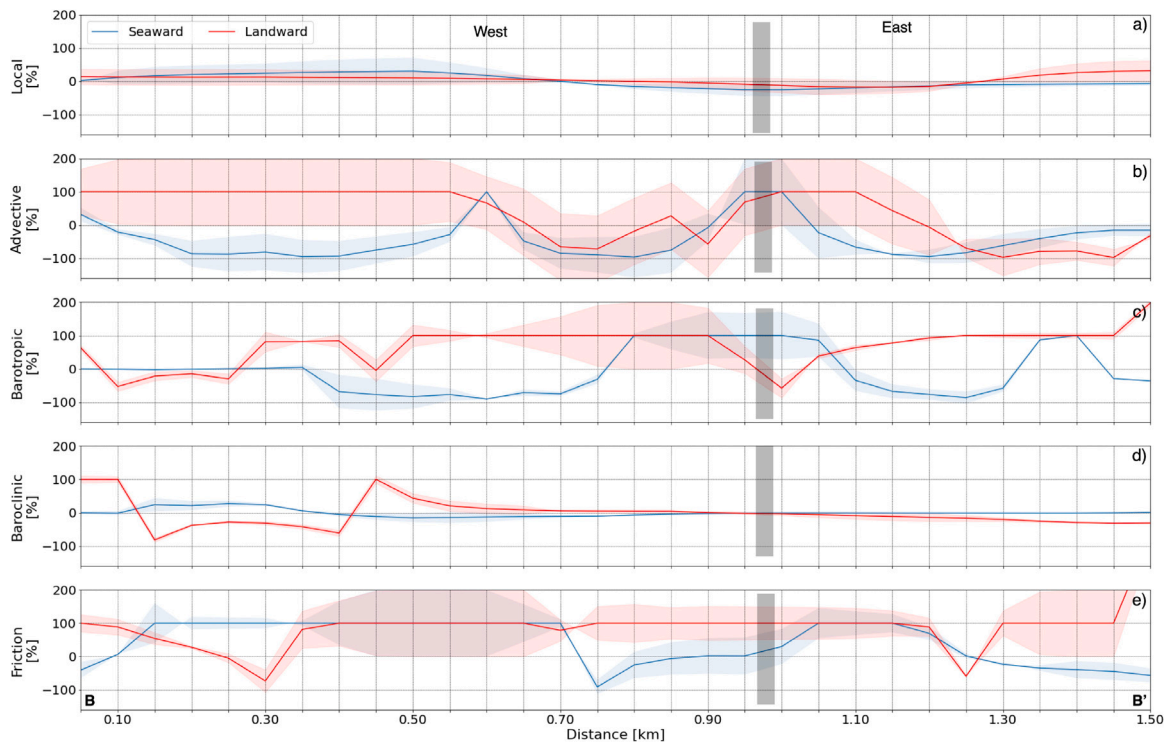

Fig. 4. As in Fig. 3, except for the Seaward (blue) and Landward (red) cross-channel profile.
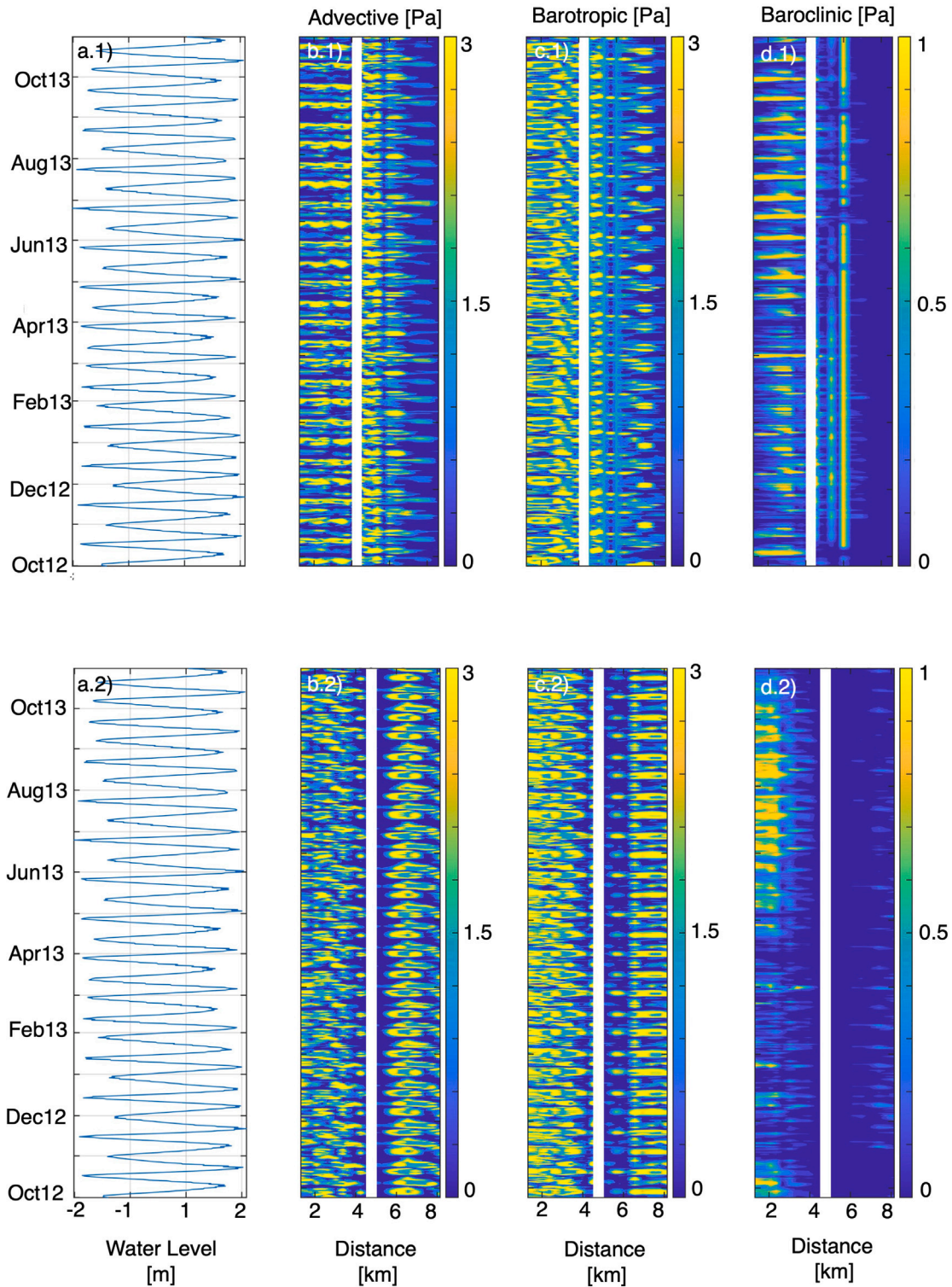
Fig. 5. Panel a shows the time series of mean sea level filtered each spring and neap tide cycle. Panels b-d correspond to the pressure terms of the momentum equation (advection, barotropicity and baroclinicity, respectively) for the along-channel profiles including the pile. The vertical white rectangle locates the bridge piling. Rows 1 and 2 show the West and East profiles, respectively.

and mostly located in the outer basin and at the connection with the Puntales Channel. In the along-channel profile West (Fig. 5d.1) there is a rise in the Landward value. As seen in Zarzuelo et al. (2021, 2022), the baroclinicity dominates in highly frictional areas, impacting stratification and sediment transport. Furthermore, regarding the

baroclinicity, it can be observed how the most significant changes occur during the summer, since there is a greater heat flux. Assessing the effect of the pile, it is observed that the baroclinicity (Figs. 7–8d) undergoes a large increase with the pile (80%) in the months of spring–summer temperature increase (Feb 13–Sep 13).
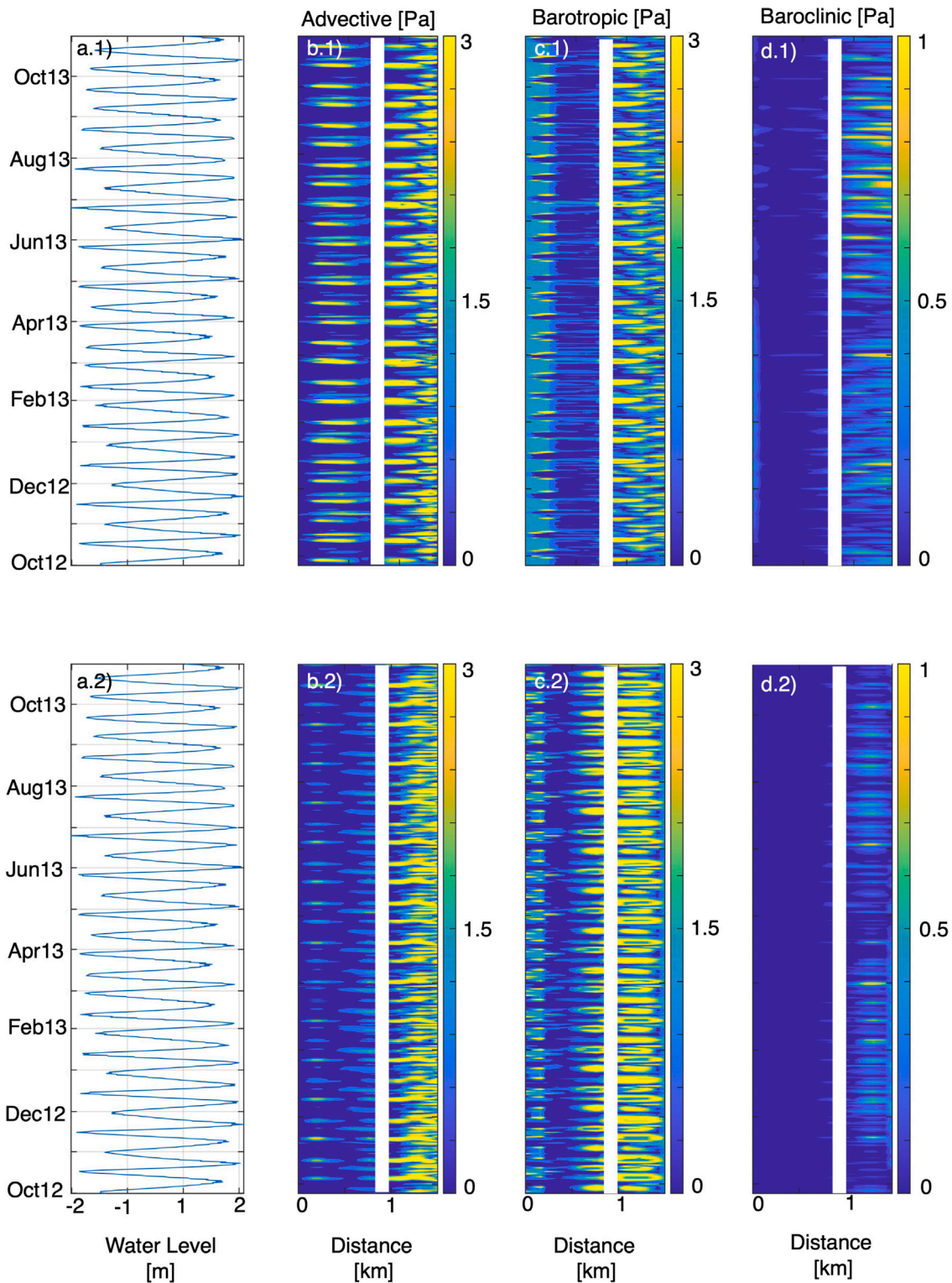
Fig. 6. As in Fig. 5, except for Seaward (1) and Landward (2) cross-channel profiles.

4.4. The role of the pile on the subtidal momentum balance

The subtidal balance is calculated as the average of each term during a tidal cycle. Considering the previous analyses, only the advective and baroclinic terms along the along-channel profiles are analyzed.

Results show increases and decreases of these residual quantities that may be related to drivers besides the fortnightly tide (Figs. 10a-b

and 11a-b for along-channel profiles West and East, respectively). Seasonal variability is clearly related to the rise and fall of the baroclinicity (b). In addition, to explore the possible response to wind forcing, two points have been selected, one Seaward (yellow) and one Landward (purple), in the areas most affected by the construction of the bridge pile. Both advection and baroclinicity decrease at the Seaward point and increase at the Landward point in the along-channel profile West (Fig. 10c-d). In the along-channel profile East, the baroclinicity shows
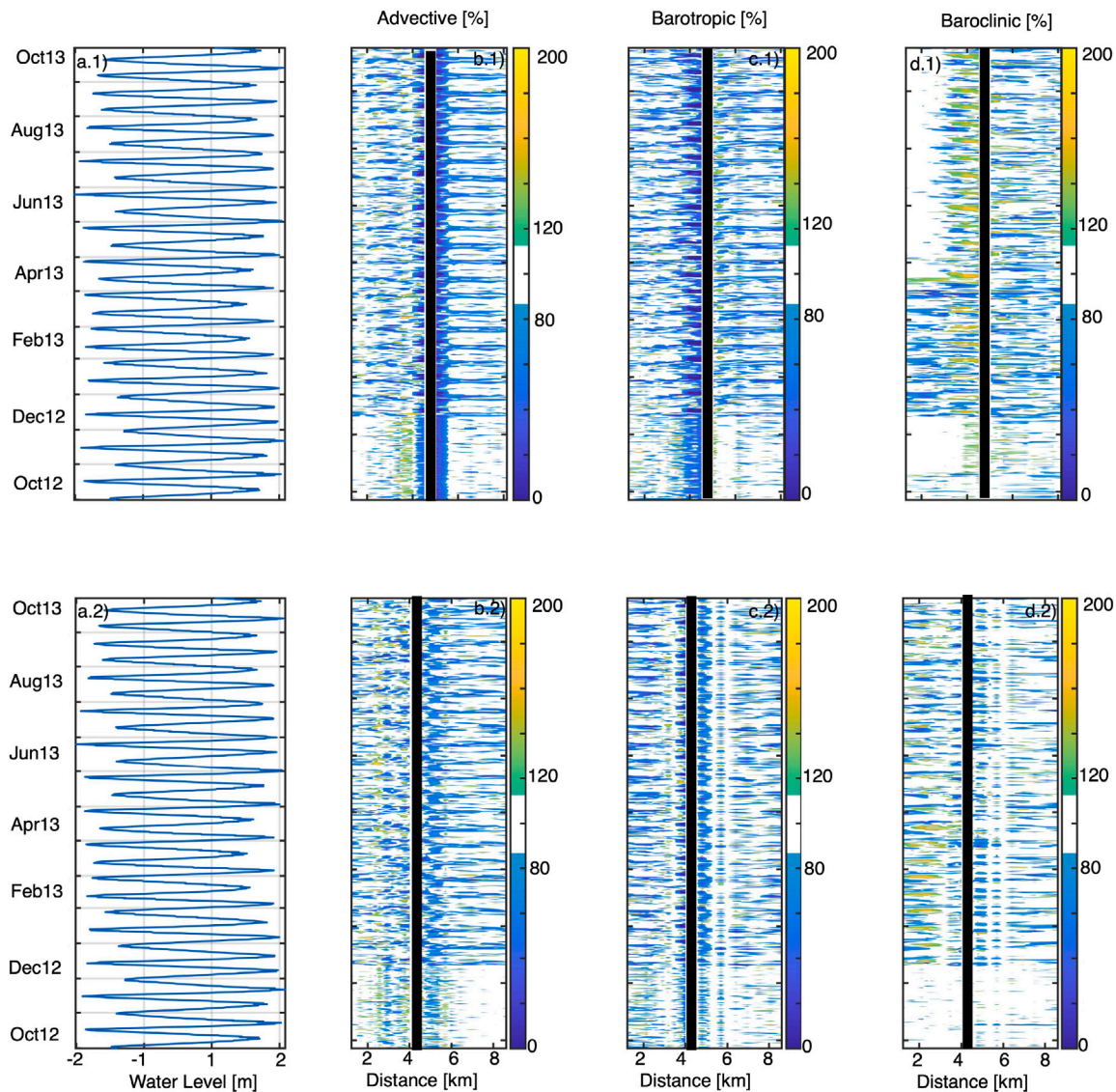
Fig. 7. As in Fig. 5, except for the differences between case with and without pile (with/without · 100). Black rectangle locates the bridge piling. White color corresponds to no changes. Yellow to green (light to dark blue) correspond to an increase (decrease) due to the pile.

the same as on the West (Fig. 11d). However, the advective term in the East has equivalent Seaward and Landward values (Fig. 11c). With wind speeds ≥ 5 m/s the advective term (c) decreases, especially with westward winds (Nov12, Sep13), as well as the baroclinicity (d) along both along-channel profiles. On the contrary, with eastward winds, both terms increase (middle of Jun13 and Sep13). Finally, the increase in the baroclinicity (mainly Seaward) during the period May13–Sep13 is again remarkable. Thus, baroclinicity is influential at the Landward point in the along-channel profile East (Fig. 11d), as the values are higher than in the along-channel profile West (Fig. 10d). Baroclinicity is more important on the East than on the West, possibly due to the depth and the tidal-flat flow from the adjacent area.

The effects of the pile are determined by comparing dynamic terms for the case with and without pile. In the along-channel profile West, changes in advection (Fig. 10c, 50% lower with pile) are seen in the peaks below 1.5 Pa, these being obtained with eastward winds above 5 m/s (Mar13–May13). However, the effect of the pile seems to diminish during maximum peaks (Nov12) with westward winds. With mean westward velocities (Jul13) the changes are noticeable (30% lower with the pile), as well as with strong eastward velocities (Nov12 and Dec12) for the baroclinicity (Fig. 10d). The changes are more noticeable (50% lower with pile) with eastward winds (Jun13,

Aug13), for the baroclinicity (Fig. 10d). In the along-channel profile East, when the winds come from the east, there is an increase (30%) of the baroclinicity (Sep13, Fig. 11d) with the pile; however, when the wind is westward the term decreases (10%) (May13- Fig. 11d). The advective term (Fig. 11) follows the same pattern as baroclinicity, although the changes are more complex as it does not follow any defined pattern.

5. Discussion

As presented in Section 4.1, the most important terms are advection and barotropicity, which are at least twice as high as the rest (Fig. 3). In contrast to most estuarine environments, the barocline contribution is one order of magnitude smaller than the barotropic. This is due to the low freshwater input (< 20 m^3/s), and the rapid mixing of the bay, similar to the St. Augustine inlet (Tutak and Sheng, 2011). The forcing that causes the largest temporal changes of the terms is the tide, and these changes occur mainly in the advective and barotropic terms. However, a positive correlation is found between baroclinicity and atmospheric temperature and solar radiation during summer. Summer conditions favor a greater difference in salinity and temperature between the inside and outside of the bay.
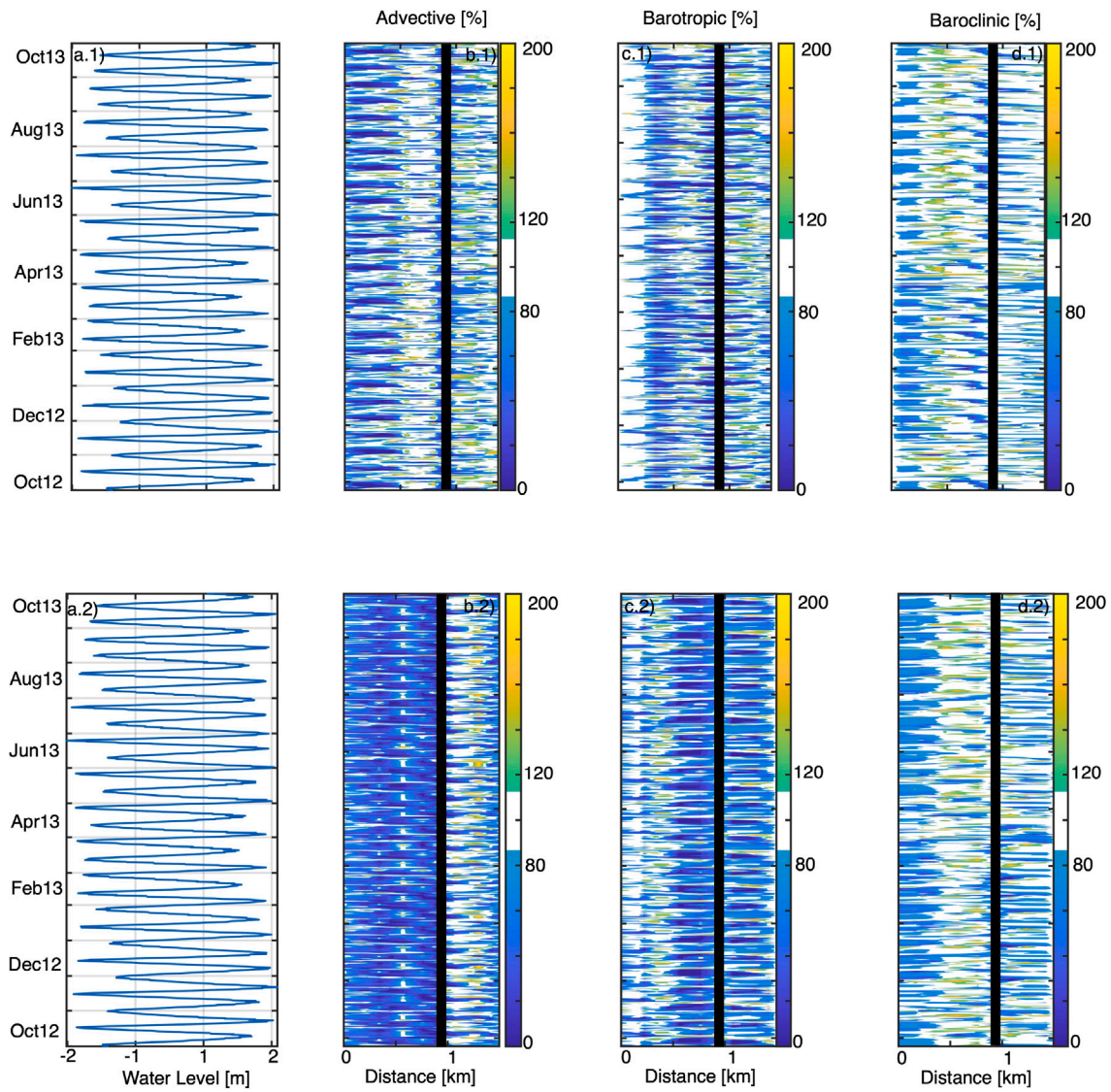
Fig. 8. As in Fig. 6, except for the differences between case with and without pile (with/without ·100). Black rectangle locates the bridge piling. White color corresponds to no changes. Yellow to green (light to dark blue) correspond to an increase (decrease) due to the pile.
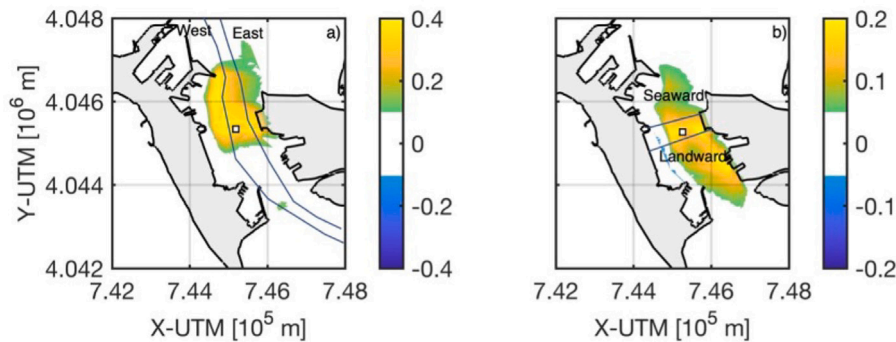

Fig. 9. Differences of the projected velocity over the channel axis at the surface (v_{pile} - v_{Nopile}) for the maximum flood (a) and maximum ebb (b) recorded during the simulated period (October 2012–October 2013). The rectangle corresponds to the bridge pile.

In the along-channel profile, the local and barotropicinity are balanced by the advection, baroclinicity and friction over the Seaward zone. However, near the pile, only advection and barotropicity play an important role, counterbalanced by friction. The same effect was shown by Alahmed et al. (2021), who observed a reduction of the

barotropic gradient in estuarine zones with higher depths. Over the Landward zone, the behavior is similar to what is observed for the Seaward with the difference that the baroclinicity loses importance in favor of friction. In both longitudinal profiles, the baroclinicity gains importance near the pile and Landward. This could be attributed to
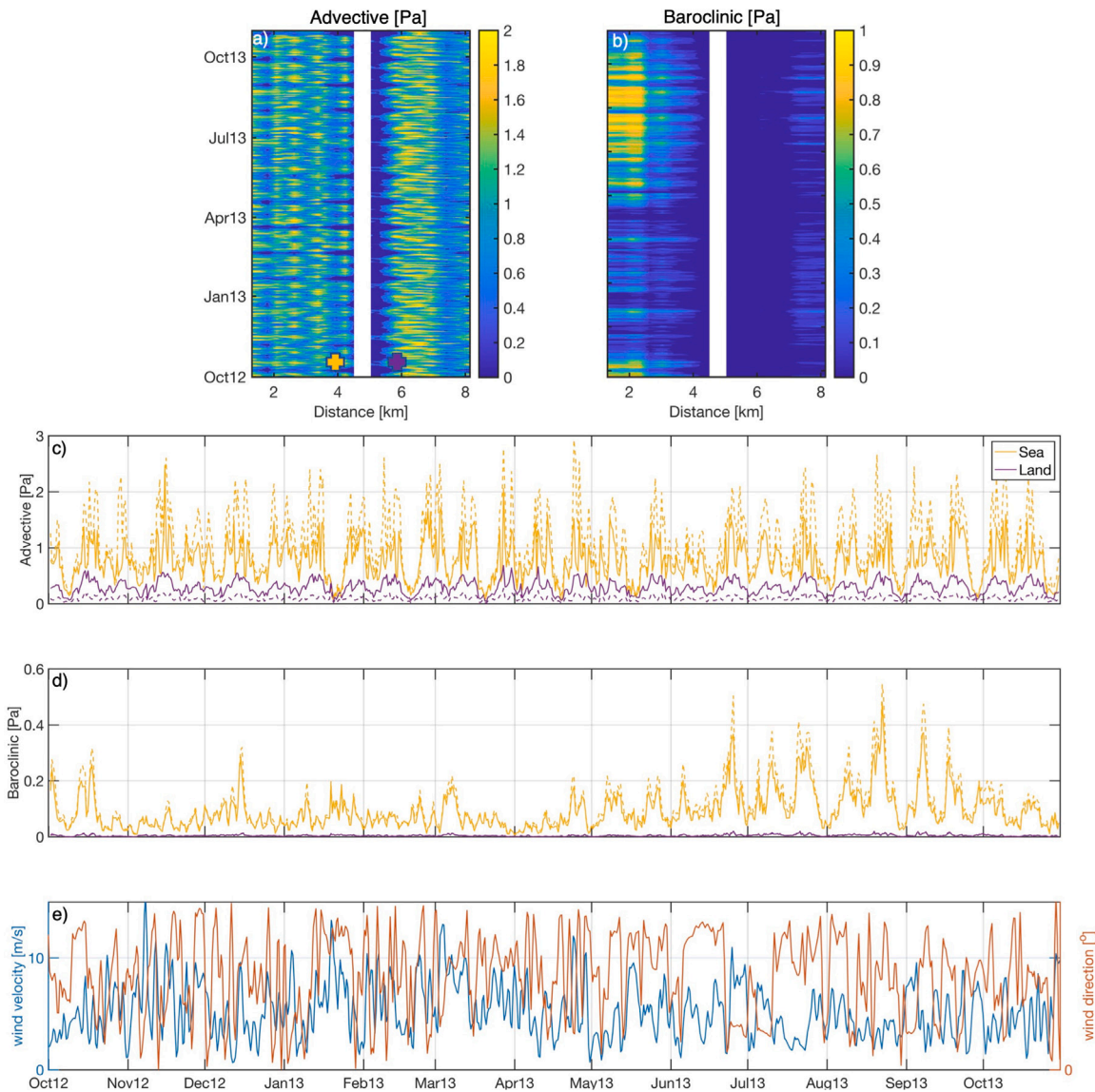
Fig. 10. Panels a and b represent the residual advective and baroclinic term, respectively. White rectangle corresponds to the bridge pile. Panels c and d represent the residual advective baroclinic term for a point (yellow and purple crosses panel a and b), respectively. Solid line with pile and dash line without pile. Panel e wind velocity (blue line) and direction (orange line) for the simulation year. This figure corresponds to the along-channel profile West.

baroclinicity sensitivity to depth. When compared to the no-pile case, the largest changes are produced in the advective, barotropic and baroclinic terms, changing the distribution of densities. They are all concentrated around the same value in the no-pile case while being more distributed in the pile case (blue). This distribution could lead to greater sediment mobilization and water exchange, as these are the mechanisms resulting from stronger tidal flow (Gatto et al., 2017). The changes produced in the West profile reach up to 1.7 km Seaward and 1.0 km Landward, and for the East profile 1.8 km Seaward and 1.4 km Landward (yellow squares, Fig. 4).

In Section 4.2 it has been concluded that the main mechanism of the advective, barotropic and baroclinic term is the tide (being in the barotropicity the only driver). However, the advective and baroclinic term are affected by seasonality and wind-driven as seen in Sections 4.3 and 4.4, respectively. It was concluded that spring tides increase these terms close to the pile, whereas in neap tides higher values are also reached in the areas close to the margins (Figs. 5 and 6). If the pile is included, the advection decreases (50%) in the deeper areas, where higher velocities are found (Zarzuelo et al., 2015, 2017). On the contrary, for the barotropicity, the most significant changes (60%

reduction) are found in the areas adjacent to the pile and in the outer basin; this can be due to the decrease in the sea level due to the constriction. These effects may be related to the turbulent intensity (Fig. 12a). It has been observed that the turbulent intensity increases significantly around the obstacle (30%), up to a distance of 800 m both Seaward and Landward. It also maintains significant fluctuations in the velocity field, which indicates that vortices starts developing (Fig. 12c) Grashorn and Stanev (2016).

The importance of seasonal variability should be emphasized (Section 4.3). Results show that the highest baroclinic values are obtained in the warmest months (May 13–Sep 13, Figs. 10d and11d). It is during these months, in combination with westerly–easterly winds (studied in Section 4.4), when more significant changes in the baroclinicity are observed and may affect the stratification (as Scully, 2016; Palmer et al., 2019). To show the importance of the stratification, the SIPS number is calculated (Fig. 12b) during summer (for the rest of seasons, see Supplementary). Three zones can be differentiated in the outer and Puntales Channel: (1) the zone closest to San Pedro estuary (with freshwater discharge) where the flow is stratified (yellow); (2) the navigation channel where the SIPS regime predominates (light green);
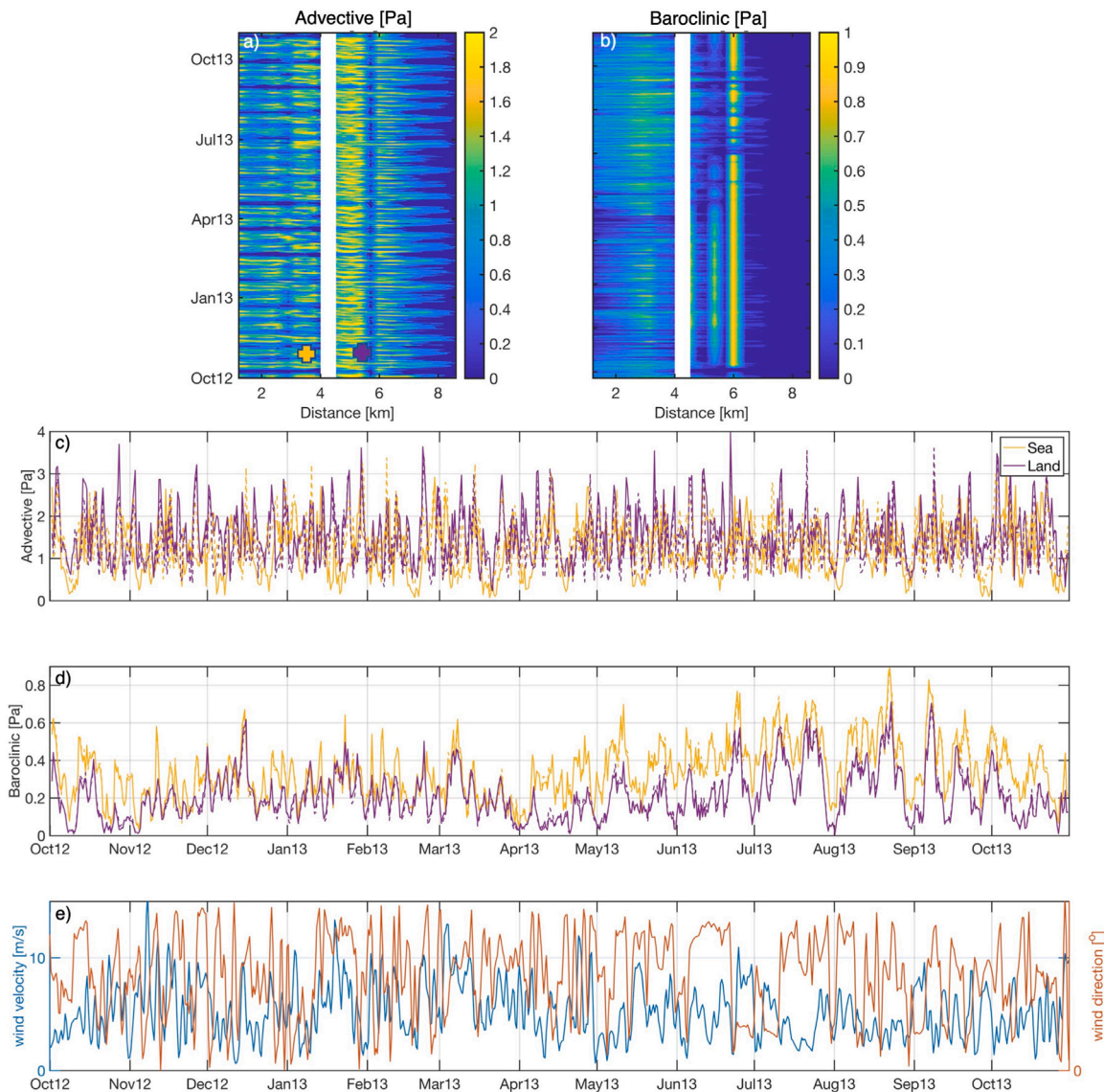
Fig. 11. As in Fig. 10, except for along-channel profile East.

and (3) the shallowest well-mixed (dark green) zone of the Puntales Channel. So, it can be agreed that the pile impacts the SIPS zonation, shifting the SIPS regime to the shallower zones and enlarging the stratified zones. The completely well-mixed zones are not altered, as seen in Cazenave et al. (2016). With the pile (Fig. 12d), it is observed that the regime shifts from SIPS to stratified (green) in the east margin and from SIPS to well mixed (blue) in the west margin. This implies less mixing on the east margin, possibly caused by decreasing inflow, and more mixing on the west margin due to higher velocities. These findings are in agreement with the experimental analyses by Grashorn and Stanev (2016), Williams and Stacey (2016), which demonstrated in a similar study area that construction works (such as obstacles) result in changes in the circulation, tidal regime, sediment pattern and even biogeochemical systems.

Finally, both the methodology and the results of this study can be implemented at other sites where interventions are carried out that also pose an obstacle to the natural behavior of the system. The most relevant specific cases are offshore wind farms and wave and tidal energy converters (WECs and TECs), all of them booming in recent times and expected to increase in the coming years.

6. Conclusion

The aim of this work was to determine the impact of the bridge piling on the local dynamics of the Bay of Cádiz. The study also determined the effects produced by the bridge piling under forcings such as tides, winds and seasonal variability. For this purpose, an area of interest has been defined inside the bay, the Puntales Channel and its connection with both inner and outer basins, and specifically two along-channel profiles and two cross-channel profiles have been established to quantify these changes. These profiles cover the areas adjacent to the bridge piling where changes were expected.

The advection and barotropicity have the greatest influence on the momentum balance equation, dominating throughout the simulation period. However, baroclinicity is one order of magnitude smaller than the above terms. With the construction of the pile, these two terms are modified up to 1 km Landward on the east margin and up to 2 km Seaward on the west margin, with the greatest changes found at a distance of 0.5 km from the pile, occupying an area of 2.5 km^2 both Seaward and Landward of the pile. The barotropicity is most altered Landward of the pile in the eastern section, being the fortnightly
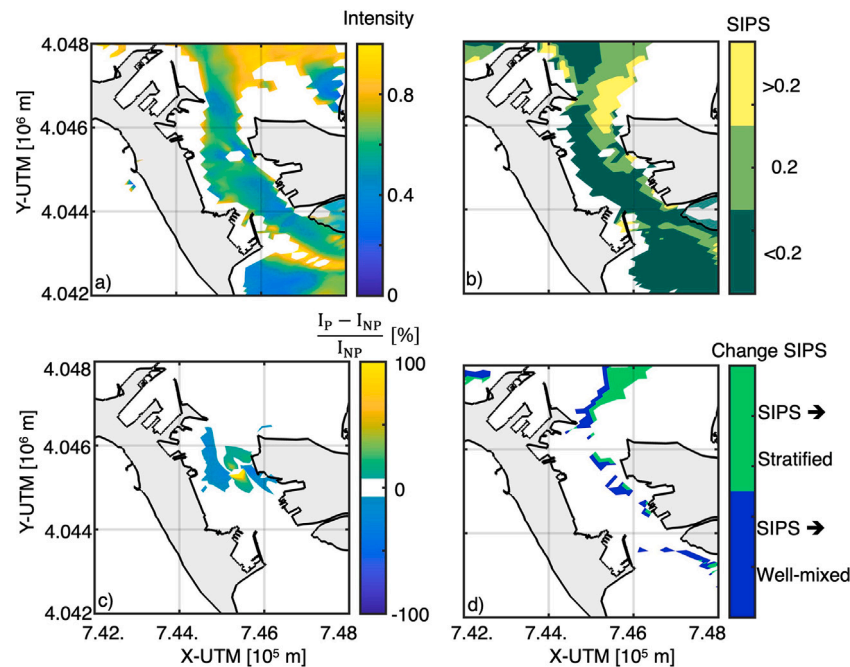
Fig. 12. For the simulation with pile: Panel (a) time-averaged for the simulation period of turbulence intensity and panel (b) Simpson's number for the summer of the simulated year. The difference between the simulation with and without pile of turbulence intensity and Simpson's number are shown in panels c and d, respectively.

variation the unique driver. The largest changes in the advective and baroclinicity are found Landward during spring tide and ebb periods, and Seaward during neap tide and flood periods.

Another mechanism that modifies the behavior of the baroclinicity and advection is buoyancy forcing. In summer, the baroclinicity increases up to 40%. Furthermore, with the construction of the pile, changes are observed in the summer months, where there is a Landward reduction with easterly winds and a Seaward reduction with westerly winds. The wind also modifies the advective behavior, where westerly winds amplify the Seaward value and the Landward value decreases. Conversely, easterly winds amplify the Landward value and the Seaward value decreases. Thus, a westerly wind coinciding with a flood period amplifies the Seaward advection by mixing the water (shallower zone), and easterly winds coinciding with an ebb period amplify the Landward advection by mixing the water more (deeper zone).

CRediT authorship contribution statement

Carmen Zarzuelo: Conceptualization, Methodology, Numerical modeling, Writing – original draft, Software, Data Curation, Formal analysis, Investigation, Review & editing. **Arnoldo Valle-Levinson:** Investigation, Writing – original draft. **Alejandro López-Ruiz:** Conceptualization, Writing – original draft, Supervision, Software, Formal analysis, Investigation, Review & editing. **Manuel Díez-Minguito:** Investigation, Writing – original draft. **Miguel Ortega-Sánchez:** Conceptualization, Writing – original draft, Supervision, Funding acquisition, Review & editing.

Declaration of competing interest

The authors declare that they have no known competing financial interests or personal relationships that could have appeared to influence the work reported in this paper.

Data availability

Data will be made available on request.

Appendix A. Supplementary data

Supplementary material related to this article can be found online at https://doi.org/10.1016/j.oceaneng.2023.113746.

References

Alahmed, S., Ross, L., Sottolichio, A., 2021. The role of advection and density gradients in driving the residual circulation along a macrotidal and convergent estuary with non-idealized geometry. Cont. Shelf Res. 212, 104295.

Burchard, H., Hetland, R.D., 2010. Quantifying the contributions of tidal straining and gravitational circulation to residual circulation in periodically stratified tidal estuaries. J. Phys. Oceanogr. 40 (6), 1243–1262.

Cazenave, P.W., Torres, R., Allen, J.I., 2016. Unstructured grid modelling of offshore wind farm impacts on seasonally stratified shelf seas. Prog. Oceanogr. 145, 25–41.

De Jonge, V., 1992. Tidal flow and residual flow in the ems estuary. Estuar. Coast. Shelf Sci. 34 (1), 1–22.

Dong, C., McWilliams, J.C., 2007. A numerical study of island wakes in the Southern California Bight. Cont. Shelf Res. 27 (9), 1233–1248.

Dong, C., McWilliams, J.C., Shchepetkin, A.F., 2007. Island wakes in deep water. J. Phys. Oceanogr. 37 (4), 962–981.

Dorrell, R., Lloyd, C., Lincoln, B., Rippeth, T., Taylor, J., Caulfield, C.-c., Sharples, J., Polton, J., Scannell, B., Greaves, D., et al., 2022. Anthropogenic mixing of seasonally stratified shelf seas by offshore wind farm infrastructure. Front. Mar. Sci. 9, 1–125.

Egbert, G.D., Erofeeva, S.Y., 2002. Efficient inverse modeling of barotropic ocean tides. J. Atmos. Ocean. Technol. 19 (2), 183–204.

Fernández-Fernández, S., Ferreira, C.C., Silva, P.A., Baptista, P., Romão, S., Fontán-Bouzas, Á., Abreu, T., Bertin, X., 2019. Assessment of dredging scenarios for a tidal inlet in a high-energy coast. J. Mar. Sci. Eng. 7 (11), 395.

Flórez-Orrego, D., Arias, W., López, D., Velásquez, H., 2012. Experimental and CFD study of a single phase cone-shaped helical coiled heat exchanger: an empirical correlation. In: Proceedings of the 25th International Conference on Efficiency, Cost, Optimization, Simulation and Environmental Impact of Energy Systems. pp. 375–394.

Fringer, O., Gerritsen, M., Street, R., 2006. An unstructured-grid, finite-volume, nonhydrostatic, parallel coastal ocean simulator. Ocean Model. 14 (3–4), 139–173.

Gatto, V.M., van Prooijen, B.C., Wang, Z.B., 2017. Net sediment transport in tidal basins: quantifying the tidal barotropic mechanisms in a unified framework. Ocean Dyn. 67 (11), 1385–1406.

Geyer, W.R., MacCready, P., 2014. The estuarine circulation. Annu. Rev. Fluid Mech. 46 (1), 175–197.

Grashorn, S., Stanev, E.V., 2016. Kármán vortex and turbulent wake generation by wind park piles. Ocean Dyn. 66 (12), 1543–1557.

Hamilton, P., 1990. Modelling salinity and circulation for the Columbia River Estuary. Prog. Oceanogr. 25 (1–4), 113–156.

Janzen, C.D., Wong, K.-C., 2002. Wind-forced dynamics at the estuary-shelf interface of a large coastal plain estuary. J. Geophys. Res.: Oceans 107 (C10), 3138.

Jay, D.A., Smith, J.D., 1990. Circulation, density distribution and neap-spring transitions in the Columbia River Estuary. Prog. Oceanogr. 25 (1–4), 81–112.

Juarez, B., Valle-Levinson, A., Li, C., 2020. Estuarine salt-plug induced by freshwater pulses from the inner shelf. Estuar. Coast. Shelf Sci. 232, 106491.

King, R., Johns, D., 1976. Wake interaction experiments with two flexible circular cylinders in flowing water. J. Sound Vib. 45 (2), 259–283.

Lai, Z., Chen, C., Cowles, G.W., Beardsley, R.C., 2010. A nonhydrostatic version of FVCOM: 1. Validation experiments. J. Geophys. Res.: Oceans 115 (C11).

Lass, H., Mohrholz, V., Knoll, M., Prandke, H., 2008. Enhanced mixing downstream of a pile in an estuarine flow. J. Mar. Syst. 74 (1–2), 505–527.

Lloret, J., Turiel, A., Solé, J., Berdalet, E., Sabatés, A., Olivares, A., Gili, J.-M., Vila-Subirós, J., Sardá, R., 2022. Unravelling the ecological impacts of large-scale offshore wind farms in the Mediterranean Sea. Sci. Total Environ. 824, 153803.

Mahadevan, A., Oliger, J., Street, R., 1996a. A nonhydrostatic mesoscale ocean model. Part I: Well-posedness and scaling. J. Phys. Oceanogr. 26 (9), 1868–1880.

Mahadevan, A., Oliger, J., Street, R., 1996b. A nonhydrostatic mesoscale ocean model. Part II: Numerical implementation. J. Phys. Oceanogr. 26 (9), 1881–1900.

Marshall, J., Hill, C., Perelman, L., Adcroft, A., 1997. Hydrostatic, quasi-hydrostatic, and nonhydrostatic ocean modeling. J. Geophys. Res.: Oceans 102 (C3), 5733–5752.

Miller, J.L., Valle-Levinson, A., 1996. The effect of bridge piles on stratification in lower Chesapeake Bay. Estuaries 19 (3), 526–539.

Nepf, H., Geyer, W., 1996. Intratidal variations in stratification and mixing in the Hudson estuary. J. Geophys. Res.: Oceans 101 (C5), 12079–12086.

Palmer, K., Watson, C., Fischer, A., 2019. Non-linear interactions between sea-level rise, tides, and geomorphic change in the Tamar Estuary, Australia. Estuar. Coast. Shelf Sci. 225, 106247.

Pisacane, G., Sannino, G., Carillo, A., Struglia, M.V., Bastianoni, S., 2018. Marine energy exploitation in the mediterranean region: steps forward and challenges. Front. Energy Res. 6, 109.

Scully, M.E., 2016. Mixing of dissolved oxygen in Chesapeake Bay driven by the interaction between wind-driven circulation and estuarine bathymetry. J. Geophys. Res.: Oceans 121 (8), 5639–5654.

Seas, U.R., Plans, A., 2011. Percentage of total population living in coastal areas.

Simpson, J.H., Brown, J., Matthews, J., Allen, G., 1990. Tidal straining, density currents, and stirring in the control of estuarine stratification. Estuaries 13 (2), 125–132.

Stark, J., Meire, P., Temmerman, S., 2017a. Changing tidal hydrodynamics during different stages of eco-geomorphological development of a tidal marsh: A numerical modeling study. Estuar. Coast. Shelf Sci. 188, 56–68.

Stark, J., Smolders, S., Meire, P., Temmerman, S., 2017b. Impact of intertidal area characteristics on estuarine tidal hydrodynamics: A modelling study for the Scheldt Estuary. Estuar. Coast. Shelf Sci. 198, 138–155.

Stark, J., Smolders, S., Vandenbruwaene, W., 2019. Using numerical simulations to improve insight on the historical evolution of tides and morphology in the Scheldt estuary. In: E-Proceedings of the 38th IAHR World Congress.

Sumich, J.L., Morrissey, J.F., 1996. Introduction to the Biology of Marine Life. Jones & Bartlett Learning.

Thurman, H., 1981. Introductory oceanography, charles e. Merrill Pub.

Tutak, B., Sheng, Y.P., 2011. Effect of tropical cyclones on residual circulation and momentum balance in a subtropical estuary and inlet: Observation and simulation. J. Geophys. Res.: Oceans 116 (C6).

Valle-Levinson, A., Schettini, C.A., 2016. Fortnightly switching of residual flow drivers in a tropical semiarid estuary. Estuar. Coast. Shelf Sci. 169, 46–55.

Velasquez-Montoya, L., Overton, M.F., Sciaudone, E.J., 2020. Natural and anthropogenic-induced changes in a tidal inlet: Morphological evolution of Oregon Inlet. Geomorphology 350, 106871.

Wang, S., Maarten, V., Xia, J., 2011. On 3D modeling of seismic wave propagation via a structured parallel multifrontal direct Helmholtz solver. Geophys. Prospect. 59, 857–873.

Williams, M.E., Stacey, M.T., 2016. Tidally discontinuous ocean forcing in bar-built estuaries: The interaction of tides, infragravity motions, and frictional control. J. Geophys. Res.: Oceans 121 (1), 571–585.

Zarzuelo, C., D'Alpaos, A., Carniello, L., López-Ruiz, A., Díez-Minguito, M., Ortega-Sánchez, M., 2019a. Natural and human-induced flow and sediment transport within tidal creek networks influenced by ocean-bay tides. Water 11 (7), 1493.

Zarzuelo, C., Díez-Minguito, M., Ortega-Sánchez, M., López-Ruiz, A., Losada, M.Á., 2015. Hydrodynamics response to planned human interventions in a highly altered embayment: The example of the Bay of Cádiz (Spain). Estuar. Coast. Shelf Sci. 167, 75–85.

Zarzuelo, C., López-Ruiz, A., D'Alpaos, A., Carniello, L., Ortega-Sánchez, M., 2018. Assessing the morphodynamic response of human-altered tidal embayments. Geomorphology 320, 127–141.

Zarzuelo, C., López-Ruiz, A., Díez-Minguito, M., Ortega-Sánchez, M., 2017. Tidal and subtidal hydrodynamics and energetics in a constricted estuary. Estuar. Coast. Shelf Sci. 185, 55–68.

Zarzuelo, C., López-Ruiz, A., Ortega-Sánchez, M., 2019b. Evaluating the impact of dredging strategies at tidal inlets: Performance assessment. Sci. Total Environ. 658, 1069–1084.

Zarzuelo, C., López-Ruiz, A., Ortega-Sánchez, M., 2020. Beyond human interventions on complex bays: Effects on water and wave dynamics (study case Cádiz Bay, Spain). Water 12 (7), 1907.

Zarzuelo, C., López-Ruiz, A., Ortega-Sánchez, M., 2021. The role of waves and heat exchange in the hydrodynamics of multi-basin bays: The example of Cádiz Bay (Southern Spain). J. Geophys. Res.: Oceans 126 (2), e2020JC016346.

Zarzuelo, C., López-Ruiz, A., Valle-Levinson, A., Díez-Minguito, M., Ortega-Sánchez, M., 2022. Bridge-piling modifications on tidal flows in an estuary. Coast. Eng. 173, 104093.

Zhang, X., Fagherazzi, S., Leonardi, N., Li, J., 2018. A positive feedback between sediment deposition and tidal prism may affect the morphodynamic evolution of tidal deltas. J. Geophys. Res.: Earth Surface 123 (11), 2767–2783.

Zhang, Y.J., Witter, R.C., Priest, G.R., 2011. Tsunami–tide interaction in 1964 Prince William Sound tsunami. Ocean Model. 40 (3–4), 246–259.